A 13.56 MHz Multiport-Wireless-Coupled (MWC) Battery Balancer with High Frequency Online Electrochemical Impedance Spectroscopy

Ming Liu, Ping Wang, Yueshi Guan, Minjie Chen
Princeton University, Princeton, NJ, USA
Email: {ml45, pwang2, minjie}@princeton.edu, hitguanyueshi@163.com

***Abstract*—This paper presents a multi-MHz multiport-wireless-coupled (MWC) battery balancer with the capability of performing high frequency electrochemical impedance spectroscopy (EIS) to monitor the battery state-of-charge (SOC) and state-of-health (SOH). The proposed MHz MWC architecture performs EIS measurement as well as battery balancing without using extra EIS perturbation circuitry. The battery balancer operates at 13.56 MHz and can perform precise EIS measurement up to 500 kHz. The high switching frequency also eliminates the magnetic core, allowing the utilization of flexible PCB air core magnetics to miniaturize the size of the battery balancer. A 13.56 MHz MWC battery balancer with a four-port air core flexible PCB transformer is built and tested with Lithium-ion, Lithium-polymer and AA-NIMH battery packs. The experimental results matched well with commercial EIS equipment and validated the effectiveness of the MWC battery balancer.**

***Index Terms*—multiport wireless-coupled transformer, battery balancer, electrochemical impedance spectroscopy, power flow control, battery management system.**

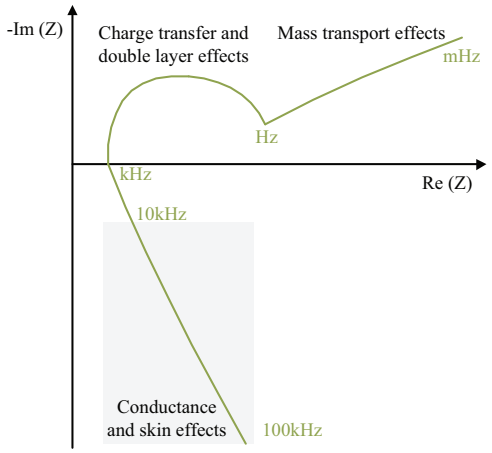

Fig. 1. A typical EIS Nyquist plot of an electrochemical battery cell.

I. Introduction

Electrochemical energy storage became increasingly important as the rapid growing of electric vehicles and renewable energy systems. Individual battery cells are usually connected in series into battery packs which can offer high output voltage and high power capacity [1]. After repeated charging and discharging, the battery cells inevitably have different state of charge (SOC) and state of health (SOH). Charge imbalance eventually leads to shorter life-cycle and reduced total battery capacity [2]. Battery balancers play important roles in monitoring battery conditions and extending the battery lifetime. In order to perform effective battery balancing and energy management, it is beneficial to identify the SOC and SOH for each battery cell. The SOC helps to identify the cells need to be charged or discharged for the battery balancer. The SOH helps to predict the remaining useful life of the cells [3].

Impedance based estimation methods, e.g., electrochemical impedance spectroscopy (EIS), are promising approaches to infer the battery SOC and SOH [4]–[7]. It is known that some of the battery balancers work as a voltage equalizer by measuring the battery voltage to estimate the SOC and balance the batteries [8]. However, the tiny voltage differences in the discharge period make it difficult to measure an accurate battery voltage for SOC estimation. The different loading conditions also highly affect the battery voltages, limiting the accuracy of the SOC estimation. Electrochemical impedance spectroscopy (EIS) is a widely-used impedance based estimation method to analyze the battery internal processes from the external measurements, i.e., the battery voltage and current [9]–[11]. By using EIS, the various electrochemical phenomena of battery can be observed and analyzed in the frequency domain. As shown in Fig. 1, the mass-transport effects can be observed at a low frequency (mHz-Hz), the charge transfer in the electrochemical double layer can be observed in a frequency range from Hz to kHz (medium frequency), and the conductance effects (physical capacitance and inductance) can be observed in the kHz and higher frequencies. In case of small batteries, e.g., the lithium batteries, much higher frequencies (10-100 kHz) are necessary to show the conductance characteristic [3].

Existing active battery balancers are usually implemented as multiport dc-link systems which utilizes dc-link capacitors to transfer energy (Fig. 2) [12]–[14]. In these balancers, the power flow between two battery cells needs to be processed by more than one "dc-ac-dc" power conversion stages. Studies on multiport ac-coupled converters exist, which can process the differential power of the two battery cells only through one dc-dc conversion stage [15], but not for frequencies above MHz. It is known that operating in the MHz range can help to eliminate the magnetic core, reduce the coil size, and improve the power density, but the electromagnetic field analysis and power flow control become challenging. Without a magnetic

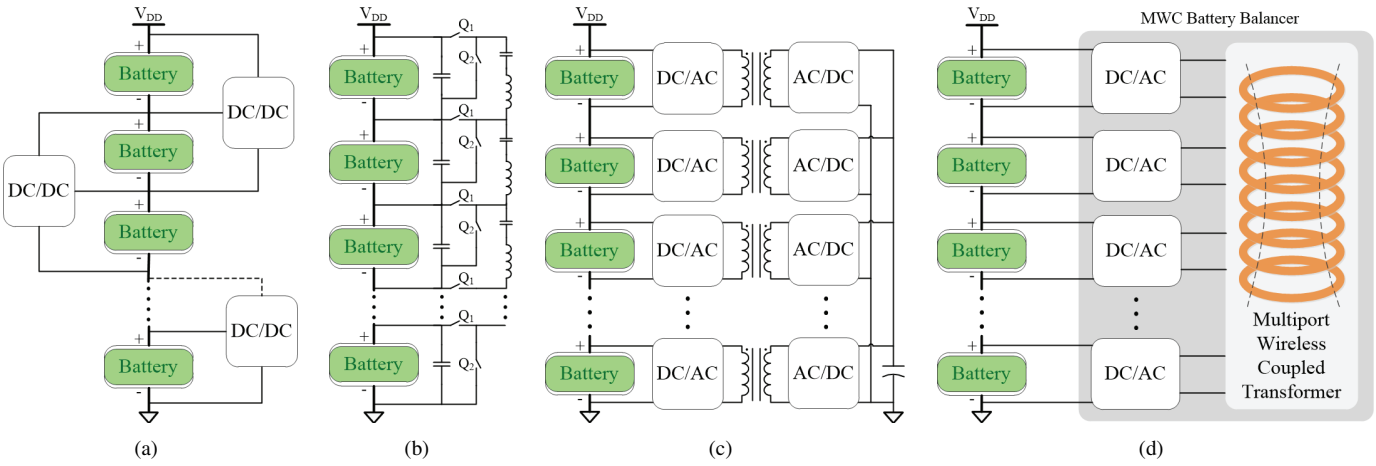

Fig. 2. Block diagrams of the battery balancing topologies. (a) Load-to-load battery balancer; (b) Switched-capacitor battery balancer; (c) Dc-coupled battery balancer; (d) Multiport wireless-coupled (MWC) battery balancer. The MWC battery balancer offer reduced power conversion stress and low component count.

core, the coupling coefficient of the coils in the MHz multiport transformer is usually much lower than that of a conventional transformer. The transformer works more like the inductive coupling coils in wireless power transfer, namely the multiport wireless-coupled (MWC) transformer.

Multi-MHz operation offers smaller size and the capability of performing high frequency EIS. There are opportunities to design a multi-MHz battery balancer to support the EIS measurement from low frequencies (mHz) to high frequencies (100kHz or higher). This paper presents a 13.56 MHz multiport wireless-coupled (MWC) battery balancer with the capability of performing EIS up to 500 kHz. The MHz MWC balancer architecture consists of multiple high frequency current mode Class-D inverters and a MWC transformer with a single "dc-ac-dc" conversion stage between two arbitrary ports, as shown in Fig. 2(d). By phase shifting the dc-ac inverters, a small-signal perturbation is created to conduct the battery EIS measurement without using extra perturbation circuitry. The multi-MHz operating frequency helps to achieve the 500 kHz EIS frequency (higher than many state-of-the-art EIS machines). The MHz frequency also helps to eliminate the magnetic core and improve the power density. A 13.56 MHz MWC battery balancer with a four-port MWC transformer is built and tested to verify the proposed approach.

II. Multi-MHz Multiport Wireless-Coupled (MWC) Battery Balancer

A. Architecture Overview

Fig. 2 shows the block diagrams of a few battery balancer designs in existing works [16]–[21]. The cell-to-cell balancing is achieved by processing the differential power among batteries. The battery balancers are usually implemented as multiport dc-link systems which utilizes dc-link capacitors to transfer energy. The power flow between two battery cells needs to be processed by more than one "dc-ac-dc" power conversion stages. The proposed multiport ac-coupled battery balancer (Fig. 2(d)) can process the differential power between two arbitrary ports through a single "dc-ac-dc" power conversion stage, which helps to improve the efficiency and reduce the component count of the battery balancer.

Compared to other dc-coupled balancer architectures, the ac-coupled battery balancer architecture can provide lower conversion stress, smaller magnetic size, and lower component count [22]. By increasing the frequency to multi-MHz, the magnetic core can be eliminated or be replaced by a very thin magnetic sheet, which will further reduce the transformer size and improve the converter power density. Furthermore, by eliminating the solid magnetic-core, the MHz multiport battery balancer can be implemented on a flexible printed circuit board (Kapton PCB). Because of the non-ideal coupling coefficient, the transformer works more like a multi-winding inductive coupling coil in wireless power transfer applications [23].

The MWC architecture shown in Fig. 2(d) can be interpreted as a multi-input-multi-output (MIMO) system connecting many sources and loads together through a single wireless-coupled linkage. In battery management application, the dc-ac converters function as current sources, which drive the multiport wireless-coupled transformer with sinusoidal current at the operation frequency. The power flow in the MWC transformer can be controlled through phase modulation [22].

B. Current Mode Class-D Inverter Design

Fig. 3 shows an example topology of the MHz MWC battery balancer. Four active current-mode Class-D inverters are wirelessly coupled through a high frequency MWC transformer. Push-pull current-mode (CM) Class D inverter is adopted to implement the dc-ac inverters due to its ground-referenced switches. Other high frequency or very high frequency inverter topologies, such as Class-E, Class-EF, Class-Φ, are also applicable. In a CM Class-D inverter, the quality-factor of the LC parallel resonant tank should be carefully designed to achieve low voltage/current harmonics and small circulating current. Fig. 4 shows the simulated waveforms of the CM Class D inverter under a varying resonance tank inductance/capacitance. Here $L_{r/t}$ is the ratio between the resonant inductance L_r and the transformer coil inductance L_t, and it is swept from 0.2 to 1 in the simulation. The

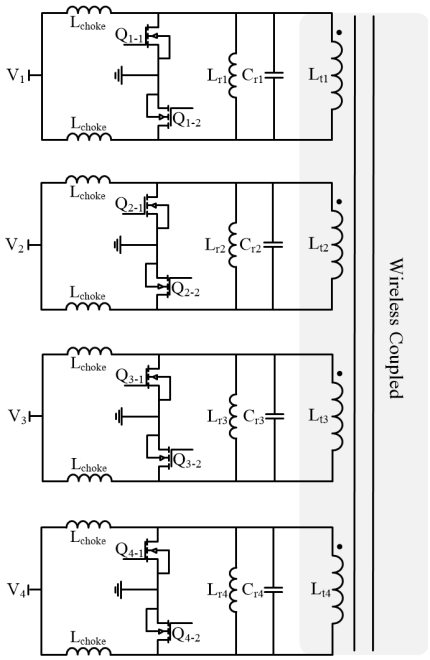

Fig. 3. An example implementation of the MHz MWC battery balancer with four current mode Class-D inverters and an air coupled transformer.

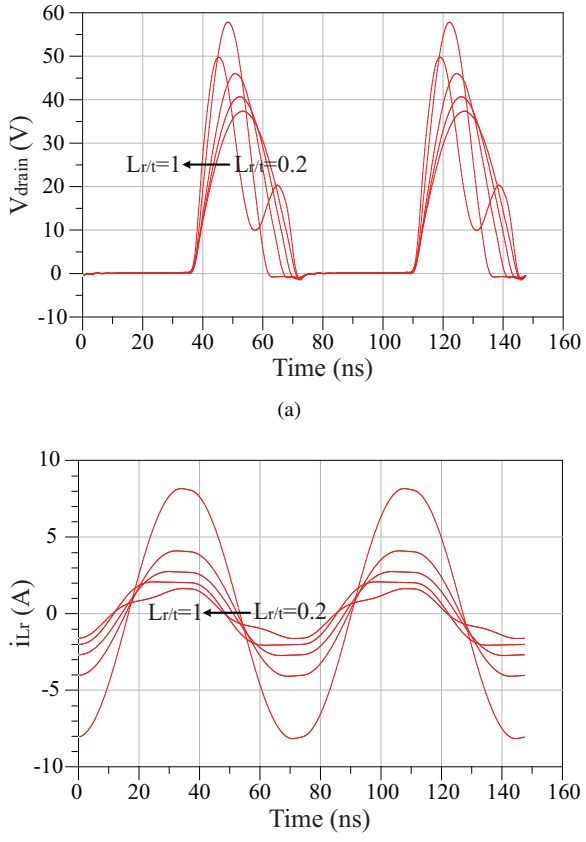

Fig. 4. Simulated waveforms of - (a) the switch drain-source voltages; and (b) the inductor circulating current - of the CM Class-D inverters.

coupling coefficients between the four coils are assumed to be identical (k=0.9) to simplify the analysis here. It can be seen that the higher $L_{r/t}$ (the higher L_r), the higher voltage/current distortion because of the lower quality factors of the resonant tank, and the lower $L_{r/t}$, the higher circulating current on L_r because of the lower impedance of the resonant tank. Based on the simulated waveforms, the inductance ratio $L_{r/t}$ can be chosen between 0.2 and 1 to avoid the high voltage/current distortion and high circulating current. And the capacitors C_{r1} - C_{r4} are designed to resonate with inductors L_{r1} - L_{r4} at the operation frequency.

C. Modeling and Control of the MIMO Power Flow

It is known that an n-port cantilever model would capture the full behavior of an n-port multi-winding transformer [24], [25] by representing a $n \times n$ impedance matrix. However, due to its topological complexity, the full-order cantilever model is not suitable to modeling and control the MIMO power flow in a MWC architecture. An alternative way to model the n-port MWC transformer is to simplify the cantilever model into an inductive coupled model, where all ports are driven by sinusoidal current source inverters. Fig. 5 shows the simplified model of a MWC transformer. The coupling between any two arbitrary coils is described by their mutual inductance. Here L_i is the self-inductance of the i^{th} coil and $L_{i,j}$ is the mutual inductance between the i^{th} and j^{th} coils. Based on this simplified cantilever model [24], the impedance matrix of the MWC transformer can be expressed as follows:

$$\begin{bmatrix} V_1 \\ V_2 \\ \cdot \\ V_n \end{bmatrix} = \begin{bmatrix} j\omega L_{1,1} & j\omega L_{1,2} & \cdots & j\omega L_{1,n} \\ j\omega L_{2,1} & j\omega L_{2,2} & \cdots & j\omega L_{2,n} \\ \cdot & \cdot & \cdots & \cdot \\ j\omega L_{n,1} & j\omega L_{n,2} & \cdots & j\omega L_{n,n} \end{bmatrix} \begin{bmatrix} i_1 \\ i_2 \\ \cdot \\ i_n \end{bmatrix}. \quad (1)$$

Note $L_{i,j}$ equals to $L_{j,i}$ in the matrix. Based on the inductive coupled model in Fig. 5 and the impedance matrix in Eq. (1), the active power feeding into port k is:

$$P_k = V_k \times i_k^* = \frac{1}{2} \sum_{q=1, q \neq k}^{n} \omega L_{k,q} I_k I_q sin\theta_{qk}. \quad (2)$$

Here i_k^* is the conjugate current of i_k. I_k and I_q are the magnitudes of the currents at port k and q, respectively. ϕ_{qk} is the phase difference between the currents of port k and q. Eq. (2) indicates that the multi-way bidirectional power flow in the multiport wireless-coupled transformer can be controlled by modulating the magnitudes and phases of all ports.

D. Modeling of the MHz MWC Transformer

As mentioned above, the coupling coefficient of the MHz MWC transformer is usually much lower than that of a conventional transformer, which affects the efficiency and power transfer capability of the battery balancer. According to Eq. (2), the power flow at a specific port k is determined by the mutual inductance between two arbitrary ports, the current amplitudes of each port, and the current phase differences between port k and all other ports. Therefore, the mutual inductance of the MWC transformer should be large enough to meet the required power transfer capability of the battery balancer. For example, in a four-port MWC battery

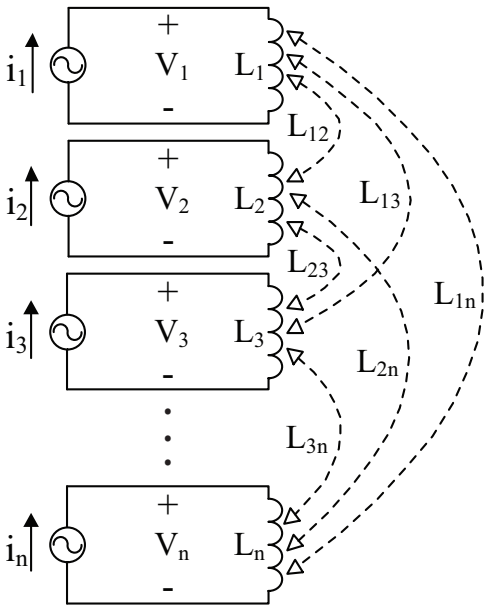

Fig. 5. Simplified lumped circuit model of the MWC transformer.

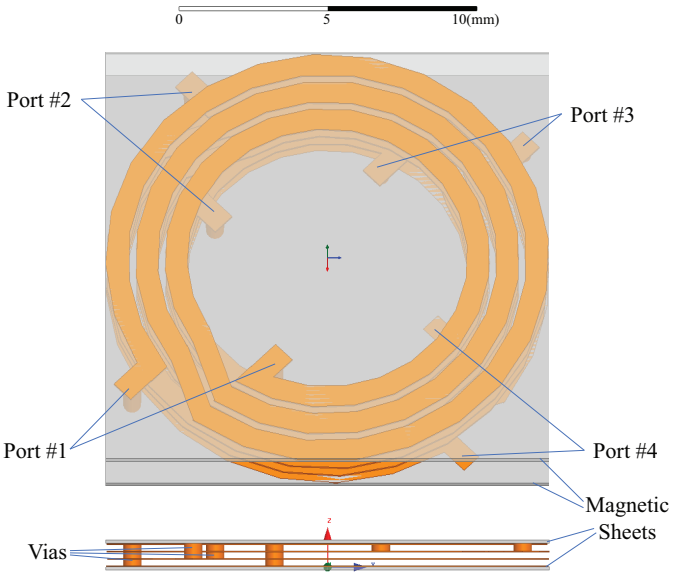

Fig. 6. 3D finite element model of an example four-port 13.56 MHz MWC transformer in ANSYS HFSS.

balancer design, the expected power flow from one Port (e.g., Port #1) to the other Port (e.g., Port #2) is about 10 W (P_{12}), and Port #3 and Port #4 are open circuited to emulate the working scenario when these ports were not used. The required mutual inductance between Port #1 and Port #2 (L_{12}) can be calculated by using Eq. (2), as shown in table I. Here the input and output currents of the Port #1 and Port #2, I_1 and I_2, are 1 A, and the phase different θ_{12} is 90°, respectively. It can be seen that for delivering 10 W from Port #1 to Port #2 the mutual inductance L_{12} should be no less than 230 nH.

Therefore, the MWC transformer should be carefully designed to achieve the required mutual inductance and the optimized coil ESR at the operation frequency, e.g., 13.56 MHz. Fig. 6 shows a finite element model (in ANSYS HFSS) of

TABLE I
REQUIRED MUTUAL INDUCTANCE FOR A 10 W RATED POWER

P_{12}	θ_{12}	I_1	I_2	ω	L_{12}
10 W	90°	1 A	1 A	13.56 MHz	230 nH

TABLE II
THE FOUR-PORT MWC TRANSFORMER PARAMETERS

n	w	g	L_{12}	L_{13}	L_{14}
3	0.75 mm	0.25 mm	321 nH	307 nH	298 nH

an example four-port MWC transformer with a 15 mm outer diameter. It consists of four coils, eight vias, and two magnetic sheets attached on top and bottom of the coil stack. The transformer can be easily implemented on flexible Kapton printed circuit board. To achieve the enough mutual inductance with a limited size (Outer diameter = 15 mm), a magnetic sheet from TDK, i.e., IBF15-100DD125X125, is used to shield the electromagnetic field. The thickness of the magnetic sheet is 0.1 mm and its relative permeability is about 150 at 13.56 MHz. By designing the number of turns (n), the trace width (w), and the trace gap (g), the coil parameters of the transformer are selected as listed in Table II. A three-turn coil with the aforementioned magnetic sheets can meet the required mutual inductance in Table I. Note a higher coil turns may cause a deceasing quality factor of the transformer. The impedance matrix of the MWC transformer with and without the soft magnetic sheets, Z_{cored} and Z_{air} are listed in Eq. (3) and (4). As expected, adding the soft magnetic sheets can significantly increase the inductance and coupling coefficient, and increase the mutual inductances between coils.

$$Z_{cored} = \begin{bmatrix} 29.5\ j\Omega & 27.4\ j\Omega & 26.2\ j\Omega & 25.4\ j\Omega \\ 27.4\ j\Omega & 28.4\ j\Omega & 26.9\ j\Omega & 26.7\ j\Omega \\ 26.2\ j\Omega & 26.9\ j\Omega & 28.3\ j\Omega & 27.2\ j\Omega \\ 25.4\ j\Omega & 26.7\ j\Omega & 27.2\ j\Omega & 28.9\ j\Omega \end{bmatrix} \quad (3)$$

$$Z_{air} = \begin{bmatrix} 12.5\ j\Omega & 10.9\ j\Omega & 9.92\ j\Omega & 9.11\ j\Omega \\ 10.9\ j\Omega & 12.3\ j\Omega & 10.9\ j\Omega & 9.92\ j\Omega \\ 9.92\ j\Omega & 10.9\ j\Omega & 12.3\ j\Omega & 10.9\ j\Omega \\ 9.11\ j\Omega & 9.92\ j\Omega & 10.9\ j\Omega & 12.3\ j\Omega \end{bmatrix} \quad (4)$$

Fig. 7 shows the simulated current distribution on the four coils of the MWC transformer. The current of each coil is evenly distributed on the surface of the coil trace. The current difference among different ports are caused by the different mutual inductances among coils.

III. HIGH FREQUENCY ONLINE ELECTROCHEMICAL IMPEDANCE SPECTROSCOPY

One unique feature of the 13.56 MHz battery balancer system is that the proposed MWC circuit can be reused to perform online electrochemical impedance spectroscopy while perform battery balancing. By modulating the phase shift at a lower frequency, a sinusoidal perturbation can be generated to conduct the battery EIS measurement without using extra

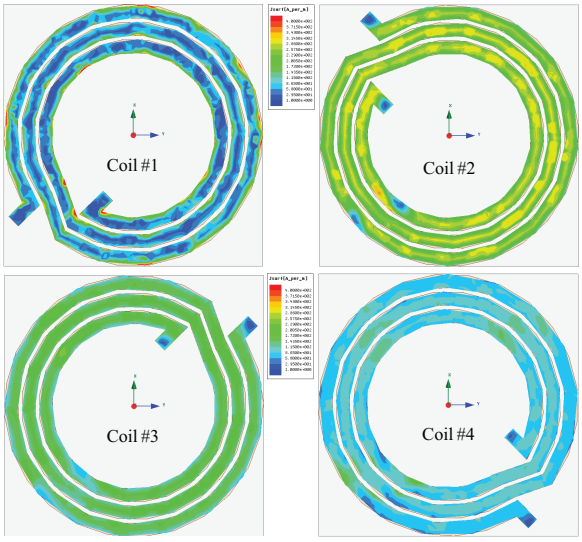

Fig. 7. Current distribution on the four coils of the MHz MWC transformer with magnetic sheets on top and bottom (simulated with ANSYS HFSS).

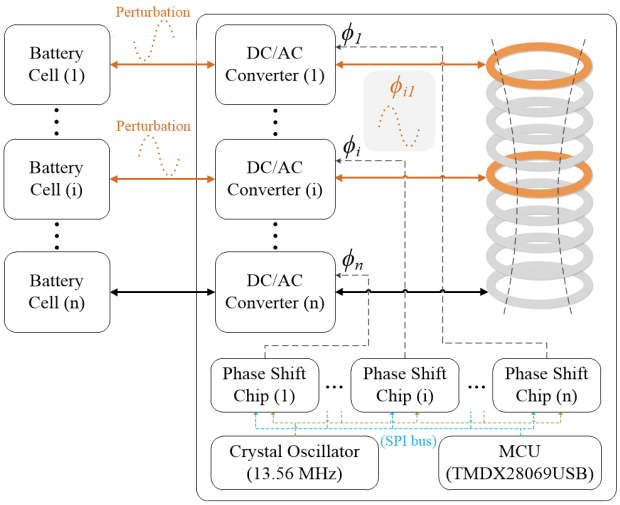

Fig. 8. Block diagram of the EIS function units in the MWC battery balancer.

power circuitry. The operation principles of the perturbation generation in the proposed battery balancer is shown in Fig. 8. For example, if battery cell #1 and battery cell #i are the targets for EIS measurement. By sweeping the difference between ϕ_1 and ϕ_i properly, a sinusoidal current can be synthesized at a range of frequencies. A commercial phase delay chip "DS1023-25" from Maxim Integrated is used to implement the phase-shift control in the balancer. A lookup table of the phase-shift values is built in a micro controller "TMDX28069USB to generate the sinusoidal perturbation at different frequencies. The desired phase-shift values are send to the multiple phase delay chips by the SPI bus.

We also developed a simple high frequency phase perturbation circuit for EIS measurement. The schematic of this simple circuit is shown in Fig. 9. The circuit consists of a crystal oscillator, a buffer, a phase perturbation circuit, and a buffer / gate driver. The oscillator provides a 13.56 MHz signal and the buffer amplifies the signal to drive the phase

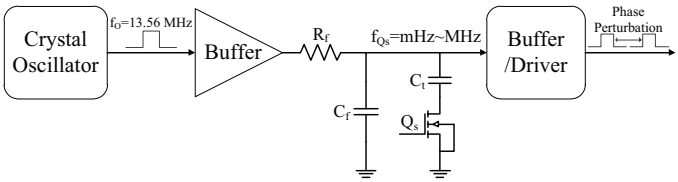

Fig. 9. A simple high frequency phase perturbation circuit for EIS.

TABLE IV
PARAMETERS OF THE FOUR-PORT MWC BATTERY BALANCER

L_1	L_2	L_3	L_4	L_{12}	L_{23}
271 nH	262 nH	267 nH	275 nH	243 nH	242 nH
L_{34}	L_{13}	L_{24}	L_{14}	L_r	C_r
243 nH	239 nH	240 nH	235 nH	110 nH	1200 pF

perturbation circuit. A switch network comprising R_f, C_f, C_t, Q_s enables the phase perturbation circuit to offer two delay options. By switching between the two delay options at a modulation frequency (e.g., 100kHz), online EIS can be performed at the modulation frequency. The perturbation frequency is determined by the switching frequency of Q_s and the duty cycle of the Q_s control signal, which is to be implemented even at very high frequencies.

Table III compares the proposed MWC architecture against a few existing works for battery online EIS. Most of the existing works require an external power supply and additional instrumentation circuit [6]–[11] to perform the online EIS. The bandwidth of the EIS is usually limited to 10 kHz or lower. The proposed MHz MWC balancer can control the power flow between multiple arbitrary ports for battery balancing and generate the high frequency perturbation for EIS. The MHz frequency of the battery balancer helps to perform wide bandwidth EIS from a few mHz to 500 kHz.

IV. Experimental Results

Fig. 10 shows a prototype four-port wireless-coupled battery balancer with multiport phase-shift control and online electrochemical impedance spectroscopy. It consists of four current-mode Class D inverters with the parallel resonant tank, a four-port MWC transformer with the flexible magnetic sheets attached on top and bottom layers, and the phase-shift control and gate drive circuits. The operation frequency is 13.56 MHz and the power rating of each port is 10 W. Eight GaN transistors, GS61004B, are used as the switches of the four CM Class D inverters. The battery balancer is built on a flexible printed circuit board with two flexible magnetic sheets on top and bottom. The entire balancer system is flexible (Fig. 10). The phase-shift and driving circuits work for both the power flow control of the battery balancing and the perturbation generation of the battery EIS. The 13.56 MHz oscillator provides the reference signal for the perturbation generation circuit and the GaN driving circuit at the same time. Table IV lists the parameters of the prototype MWC battery balancer (Fig. 3). The inductance and capacitance of the resonant tank in the CM Class-D inverters are determined based on the discussion presented in Section II-B.

TABLE III
OVERVIEW AND COMPARISON WITH EXISTING ONLINE EIS WORKS

Publication	[6]	[7]	[9]	[10]	[11]	This work
Cell Level Perturbation	No	No	No	No	Yes	Yes
Test Cell Capacity	2.6Ah	N/A	3Ah	2.3Ah	3.4Ah	3.4Ah/3Ah/2.4Ah
Perturbation Source	Load	Battery Charger	Battery Charger	Motor Controller	Active Balancer	Active Balancer
Perturbation Type	Sinusoid	Sinusoid	Sawtooth	Noise/Multisine	Sinusoid	Sinusoid/Pulse
Perturbation Current	72-750 mA	1 A	2 A	130 mA	160 mA	20-200 mA
Perturbation Bandwidth	10 kHz	100 Hz	5 kHz	2 kHz	8 kHz	500 kHz

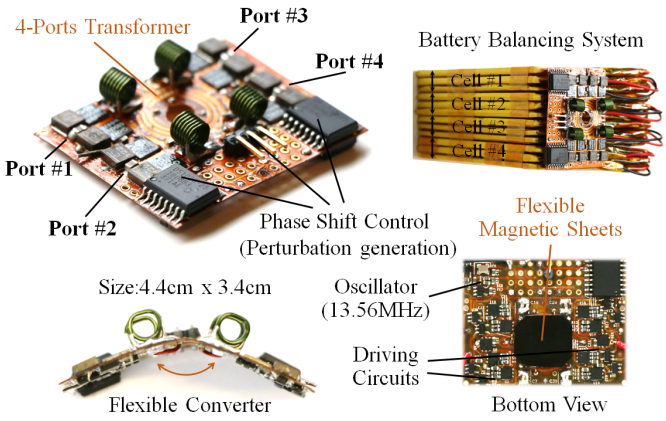

Fig. 10. A prototype four-port 13.56 MHz MWC battery balancer with multiport phase-shift control and online electrochemical impedance spectroscopy.

(a) (b) (c)

Fig. 11. Battery cells for EIS measurement: (a) a 11.1 V Lithium-ion battery pack (three 3.7 V cells in series); (b) a 11.1 V Lithium-polymer battery pack (three 3.7 V cells in series); (c) a 9.6 V AA-NIMH battery pack (eight 1.2 V cells in series). Package impedances are included in the EIS measurements.

Fig. 11 shows three different battery cells that were used in the EIS measurement. Three 3.7 V lithium-ion battery cells are series connected into a battery pack with 11.1 V battery voltage. Three lithium-polymer battery cells are also connected in series in a battery pack. Eight 1.2 V AA-NIMH cells are also connected in series to build a high voltage (9.6 V) AA-NIMH battery cell for the EIS testing.

Fig. 12 shows the power flow control and end to end efficiency of the battery balancer. The port-to-port power is controlled by modulating the phase-shift between ports. Here the current phases of the MWC transformer are controlled by adjusting the phase of the gate driving signals of the CM Class-D inverters. In this experiment, Port #1 and Port #2 are configured as the sources, Port #3 and Port #4 are configured as loads, the phases of Port #1 and Port #2 are identical and fixed at 0°, and the phases of Port #3 and Port #4

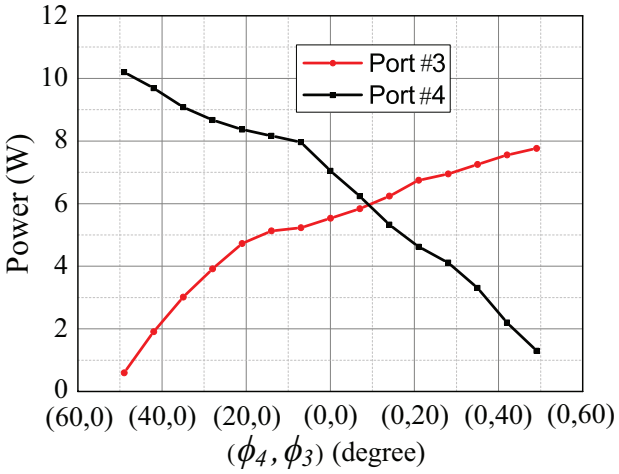

(a)

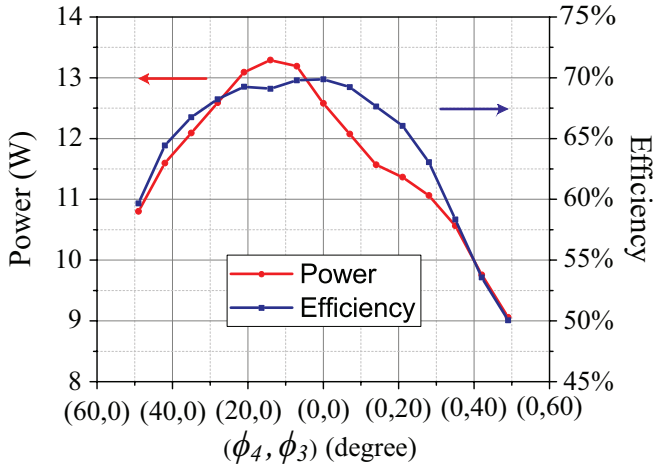

(b)

Fig. 12. Experimental results of the MWC battery balancer: (a) power flow control of the battery balancer; (b) end-to-end efficiency of the battery balancer under the power flow control.

are controlled to validate the power flow control and battery balancing operation. Here the voltages of Port #1 and Port #2 are set as 11.1 V and the voltages of Port #3 and Port #4 are set as 10 V to emulate the battery balancing scenario. As shown in Fig. 12 (a), the higher phase-shift ϕ_3 (ϕ_4), the higher power transferred to Port #3 (Port #4). For example, when ϕ_4 = 42° and ϕ_3 = 0°, the load power at Port #4 is 9.7 W and the load power at Port #3 is 1.9 W. The load powers of Port #4 and Port #3 get close when their phases are approaching each other. Fig. 12(b) shows the total load power of Port #3 and

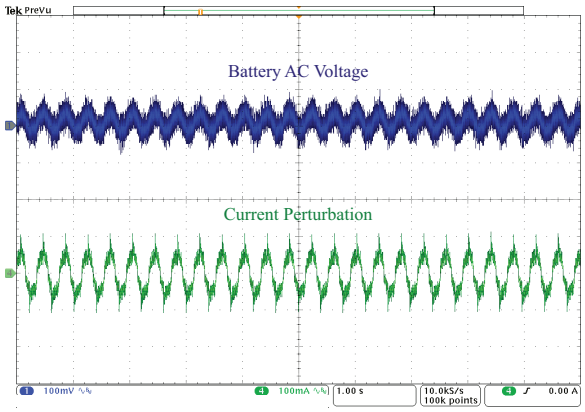

Fig. 13. Current perturbation and battery AC voltage at 2.5 Hz (1s/div).

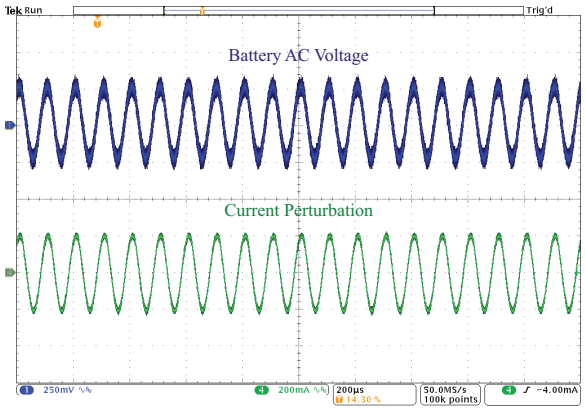

Fig. 14. Current perturbation and battery AC voltage at 10 kHz (200μs/div).

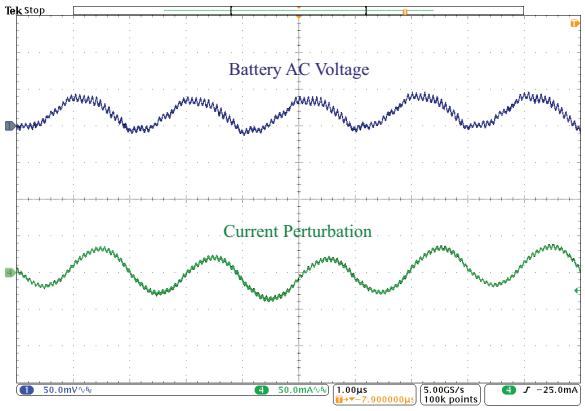

Fig. 15. Current perturbation and battery AC voltage at 500 kHz (1μs/div).

Port #4, and the end to end efficiency of the battery balancer. The peak end to end efficiency is about 70% and the main power loss is contributed by the MWC transformer due to its high coil ESRs and core loss (about 0.6 Ω with the magnetic sheets). The ESRs can be further reduced by optimizing the coil diameters and adopting better magnetic materials. Note the proposed MWC converter architecture can be also applied to multi-input-multi-output (MIMO) wireless power transfer (WPT) systems with similar modeling and design methods.

To validate the EIS capability of the proposed MWC battery balancer, the EIS experiments are conducted based on the three battery cells (Fig. 11), i.e., a lithium-ion battery pack, a lithium-polymer battery pack, and a AA-NIMH battery pack. Fig. 13, Fig. 14, and Fig. 15 show the waveforms of a 2.5 Hz,

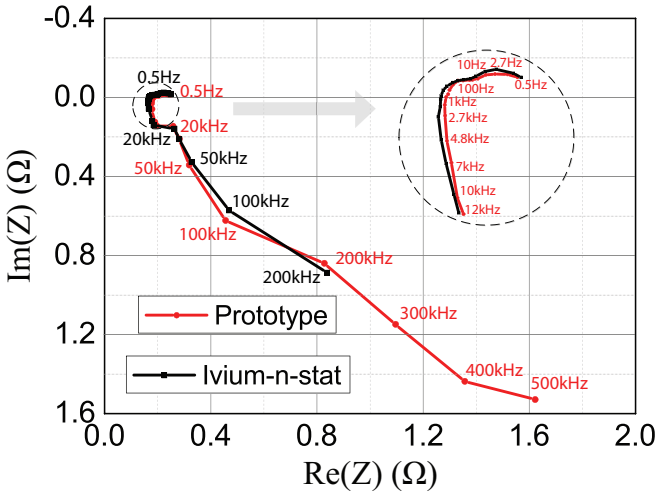

(a)

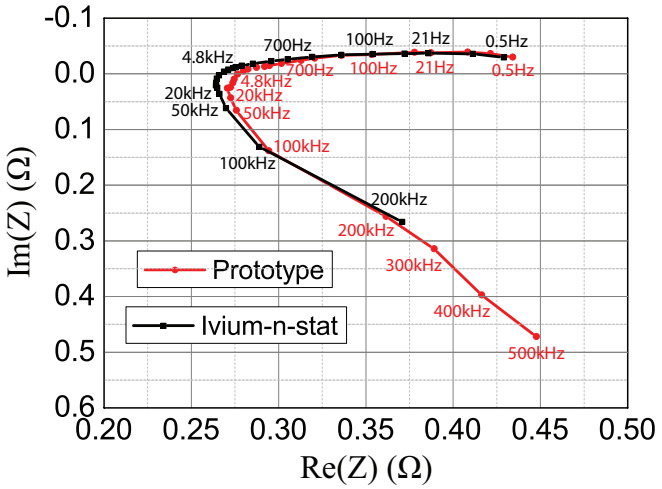

(b)

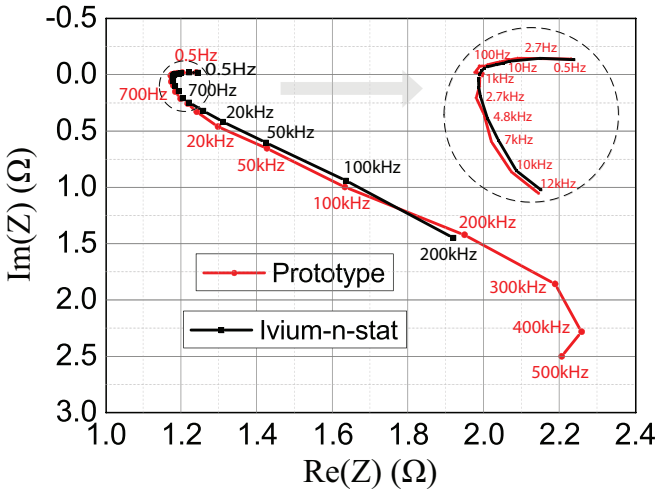

(c)

Fig. 16. EIS measurement results with: (a) Lithium-ion battery pack; (b) Lithium-polymer battery pack; (c) AA-NIMH battery pack.

a 10 kHz, and a 500 kHz current perturbations generated by the MWC battery balancer, respectively. By applying fast fourier transformation (FFT) to the measured waveforms, the fundamental components of the voltage and current can be identified, yield the cell impedance.

The EIS results measured by the MWC balancer were compared to a commercial EIS instrument, Ivium-n-Stat, manufactured by Ivium Technologies. In the experiment, the prototype MWC balancer ran 25 perturbations ranging from 500 mHz to 500 kHz on the lithium-ion battery pack, the lithium polymer battery pack, and the AA-NIMH battery pack, respectively. The Ivium-n-Stat ran 22 perturbations ranging from 500 mHz to 200 kHz on the same batteries. The maximum EIS measurement frequency of the prototype is 500 kHz. The maximum EIS measurement frequency of Ivium-n-Stat is 250 kHz. Fig. 16 compares the Nyquist plots of the three batteries measured by the MWC balancer and the Ivium-n-Stat, where good match was found. Note the battery packs used in the EIS experiment were built with series connected battery cells and the impedance of the connecting wires of the cells dominated the measured impedance at the high frequency segment of the Nyquist plots.

V. Conclusions

This paper presents a multi-MHz MWC battery balancer with online EIS measurement capability. The MHz MWC balancer architecture consists of multiple high frequency dc-ac inverters and a MWC transformer. There is only one "dc-ac-dc" conversion stage between two arbitrary ports, allowing the MWC balancer to achieve lower component count and higher power density than many other battery balancer architectures. The MHz operation of the battery balancer enables online EIS measurement for up to 500kHz as well as battery balancing without using extra power circuitry. The high frequency also helps to eliminate the magnetic core and reduce the coil size of the MWC transformer. A 13.56 MHz MWC balancer with a four-port MWC transformer is built and tested to verify the proposed approach. The EIS measurement results match well with the results measured by commertical EIS equipment.

Acknowledgment

The authors would like to thank Princeton Andlinger Center for Energy and the Environment, and the National Science Foundation (#1847365) for supporting this work.

References

[1] A. Khaligh and Z. Li, "Battery, Ultracapacitor, Fuel Cell, and Hybrid Energy Storage Systems for Electric, Hybrid Electric, Fuel Cell, and Plug-In Hybrid Electric Vehicles: State of the Art," *IEEE Transactions on Vehicular Technology*, vol. 59, no. 6, pp. 2806-2814, July 2010.

[2] L. Maharjan, T. Yamagishi, and H. Akagi, "Active-power control of individual converter cells for a battery energy storage system based on a multilevel cascade pwm converter," *IEEE Transactions on Power Electronics*, vol. 27, no. 3, pp. 1099C1107, Mar. 2012.

[3] A. Jossen, "Fundamentals of battery dynamics," *Journal of Power Sources*, vol. 154, no. 2, pp. 530-538, 2006.

[4] P. A. Cassani and S. S. Williamson, "Design, testing, and validation of a simplified control scheme for a novel plug-in hybrid electric vehicle battery cell equalizer," *IEEE Transactions on Industrial Electronics*, vol. 57, no. 12, pp. 3956C3962, Dec. 2010.

[5] W.Waag, S.Kabitz, and D.U. Sauer, "Experimental investigation of the lithium-ion battery impedance characteristic at various conditions and aging states and its influence on the application," *Applied Energy*, vol. 102, pp. 885-897,Feb. 2013.

[6] W. Huang and J. A. Abu Qahouq, "An Online Battery Impedance Measurement Method Using DC-DC Power Converter Control," *IEEE Transactions on Industrial Electronics*, vol. 61, no. 11, pp. 5987-5995, Nov. 2014.

[7] Y. Lee, S. Park and S. Han, "Online Embedded Impedance Measurement Using High-Power Battery Charger," *IEEE Transactions on Industry Applications*, vol. 51, no. 1, pp. 498-508, Jan.-Feb. 2015.

[8] F. Mestrallet, L. Kerachev, J. Crebier and A. Collet, "Multiphase Interleaved Converter for Lithium Battery Active Balancing," *IEEE Transactions on Power Electronics*, vol. 29, no. 6, pp. 2874-2881, June 2014.

[9] R. Koch, R. Kuhn, I. Zilberman and A. Jossen, "Electrochemical impedance spectroscopy for online battery monitoring - power electronics control," *16th European Conference on Power Electronics and Applications*, Lappeenranta, 2014, pp. 1-10.

[10] D. A. Howey, P. D. Mitcheson, V. Yufit, G. J. Offer and N. P. Brandon, "Online Measurement of Battery Impedance Using Motor Controller Excitation," *IEEE Transactions on Vehicular Technology*, vol. 63, no. 6, pp. 2557-2566, July 2014.

[11] E. Din, C. Schaef, K. Moffat and J. T. Stauth, "A Scalable Active Battery Management System With Embedded Real-Time Electrochemical Impedance Spectroscopy," *IEEE Transactions on Power Electronics*, vol. 32, no. 7, pp. 5688-5698, July 2017.

[12] Y. Levron, D. R. Clement, B. Choi, C. Olalla and D. Maksimovic, "Control of Submodule Integrated Converters in the Isolated-Port Differential Power-Processing Photovoltaic Architecture," *IEEE Journal of Emerging and Selected Topics in Power Electronics*, pp. 821-832, Dec. 2014.

[13] Z. Zhang, H. Gui, D. Gu, Y. Yang and X. Ren, "Hierarchical Active Balancing Architecture for Lithium-Ion Batteries," *IEEE Transactions on Power Electronics*, vol. 32, no. 4, pp. 2757-2768, April 2017.

[14] E. Candan, P. Shenoy and R. Pilawa-Podgurski, "A Series-Stacked Power Delivery Architecture With Isolated Differential Power Conversion for Data Centers," *IEEE Transactions on Power Electronics*, vol. 31, no. 5, pp. 3690-3703, May 2016.

[15] P. Wang and M. Chen, "Towards Power FPGA: Architecture, Modeling and Control of Multiport Power Converters," *IEEE Workshop on Control and Modeling for Power Electronics (COMPEL)*, Padua, 2018, pp. 1-8.

[16] A. Stillwell and R. C. N. Pilawa-Podgurski, "A resonant switched-capacitor converter with GaN transistors for series-stacked processors with 99.8% power delivery efficiency," *2015 IEEE Energy Conversion Congress and Exposition (ECCE)*, Montreal, QC, 2015, pp. 563-570.

[17] M. Liu, M. Fu, Y. Wang and C. Ma, "Battery Cell Equalization via Megahertz Multiple-Receiver Wireless Power Transfer," *IEEE Transactions on Power Electronics*, vol. 33, no. 5, pp. 4135-4144, May 2018.

[18] M. Evzelman, M. M. Ur Rehman, K. Hathaway, R. Zane, D. Costinett and D. Maksimovic, "Active Balancing System for Electric Vehicles With Incorporated Low-Voltage Bus," *IEEE Transactions on Power Electronics*, vol. 31, no. 11, pp. 7887-7895, Nov. 2016.

[19] H. Chen, L. Zhang and Y. Han, "System-Theoretic Analysis of a Class of Battery Equalization Systems: Mathematical Modeling and Performance Evaluation," *IEEE Transactions on Vehicular Technology*, vol. 64, no. 4, pp. 1445-1457, April 2015.

[20] A. M. Imtiaz and F. H. Khan, "Time Shared Flyback Converter Based Regenerative Cell Balancing Technique for Series Connected Li-Ion Battery Strings," *IEEE Transactions on Power Electronics*, vol. 28, no. 12, pp. 5960-5975, Dec. 2013.

[21] Y. Shang, B. Xia, F. Lu, C. Zhang, N. Cui and C. C. Mi, "A Switched-Coupling-Capacitor Equalizer for Series-Connected Battery Strings," *IEEE Transactions on Power Electronics*, vol. 32, no. 10, pp. 7694-7706, Oct. 2017.

[22] Y. Chen, P. Wang, H. Li and M. Chen, "Power Flow Control in Multi-Active-Bridge Converters: Theories and Applications," *IEEE Applied Power Electronics Conference and Exposition (APEC)*, Anaheim, CA, USA, 2019, pp. 1500-1507.

[23] M. Liu and M. Chen, "Dual-Band Wireless Power Transfer with Reactance Steering Network and Reconfigurable Receivers," *IEEE Transactions on Power Electronics*, to appear.

[24] R. W. Erickson and D. Maksimovic, "A multiple-winding magnetics model having directly measurable parameters," *IEEE Power Electronics Specialists Conference*, Fukuoka, 1998, pp. 1472-1478 vol.2.

[25] M. Chen, M. Araghchini, K. K. Afridi, J. H. Lang, C. R. Sullivan, and D. J. Perreault, "A Systematic Approach to Modeling Impedances and Current Distribution in Planar Magnetics," *IEEE Transactions on Power Electronics*, vol.31, no.1, pp. 560-580, January, 2016.